CrystEngComm

Isoxazolone-based Single Crystals with Large Second Harmonic Generation Effect

Journal:	*CrystEngComm*
Manuscript ID:	CE-ART-05-2015-001006.R2
Article Type:	Paper
Date Submitted by the Author:	05-Aug-2015

Complete List of Authors:	Zhang, Xinyuan; Technical Institute of Physics and Chemistry, CAS, ; University of Chinese Academy of SciencesUniversity of Chinese Academy of Sciences, Jiang, Xingxing; Technical Institute of Physics and Chemistry, Chinese Academy of Sciences, ; University of Chinese Academy of Sciences, Li, Yin; Technical Institute of Physics and Chemistry, Lin, Zheshuai; Technical Institute of Physics and Chemistry, Chinese Academy of Sciences, Zhang, Guochun; Technical Institute of Physics and Chemistry, Chinese Academy of Sciences, Wu, Yicheng; Technical Institute of Physics and Chemistry, Chinese Academy of Sciences,

Journal Name

ARTICLE

Isoxazolone-based Single Crystals with Large Second Harmonic Generation Effect †

Received 00th January 20xx,
Accepted 00th January 20xx

DOI: 10.1039/x0xx00000x

www.rsc.org/

Xinyuan Zhang,[ab] Xingxing Jiang,[ab] Yin Li,[a] Zheshuai Lin,[a] Guochun Zhang*[a] and Yicheng Wu[a]

Two nonlinear optical (NLO) crystals based on 3-phenyl-5-isoxazolone moiety, (Z)-4-(4-(dimethylamino) benzylidene)-3-phenylisoxazol-5(4H)-one ($C_{18}H_{16}N_2O_2$, DLS) and (Z)-4-(4-methoxybenzylidene)-3-phenylisoxazol-5(4H)-one ($C_{17}H_{13}NO_3$, MLS) have been successfully grown by slow evaporation method. The powder second-harmonic generation intensities of DLS and MLS are strong, about 2.8 and 1.5 times that of OH1, respectively. Such large SHG effect is further elucidated by the structure analyses and theoretical calculations. The optical and thermal properties of DLS and MLS have been characterized by UV-vis absorption spectroscopy, IR spectroscopy, thermal gravimetric analysis and differential scanning calorimetry.

Introduction

Organic nonlinear optical (NLO) crystals with large nonlinear optical susceptibility and ultrafast response time have attracted much attention because of their potential for various optical applications, such as photonic devices, optical parametric oscillation, frequency conversion, and terahertz(THz) wave generation and detection. [1, 2] In the past few decades, many organic NLO crystals were developed, including a number of pyridinium derivatives and configurationally locked polyene derivatives with D-π-A molecule construction, such as DAST, DSTMS, DASC, DASB, DSCHS, TPNS, OH1, DAV1, and MH2 etc. ‡ [3-12] In particular, DAST, DSTMS, and OH1 exhibit excellent NLO performances because of their very high NLO susceptibilities and large electro-optic (EO) coefficients and become the few commercial organic NLO crystals, which are suitable for terahertz(THz) wave generation and detection. However, the practical applications of these materials are still restricted due to the optical absorption in the working spectral region, difficulty in large size and high optical quality crystal growth, or low chemical stability.[13-15] Therefore, the search for new organic NLO materials is of extensive scientific and technological interest.

Since both microscopic higher-order susceptibility and spatial arrangement of molecules are very important to achieve large macroscopic nonlinearity, it can be an effective approach to obtain organic NLO crystal by designing molecules with suitable electron donors and electron acceptors. Among the numerous electron donors, 3-phenyl-5-isoxazolone is a simple asymmetric moiety with powerful electron withdrawing ability. D-π-A molecule used 3-phenyl-5-isoxazolone as the electron acceptor has large first molecular hyperpolarizability (*β*), which benefits to produce an intense second harmonic generation (SHG) response. [16, 17] In addition, 3-phenyl-5-isoxazolone shows a great superiority of inducing acentric packing because of its structurally asymmetric group in five-membered heterocycle. [18-20] Considering the above factors, 3-phenyl-5-isoxazolone-based compounds are likely to be good candidates for NLO materials.

Up to now, some 3-phenyl-5-isoxazolone-based compounds were found. [21, 22] In particular, the synthesis of DLS ((Z)-4-(4-(dimethylamino) benzylidene)-3-phenylisoxazol-5(4H)-one, $C_{18}H_{16}N_2O_2$)) and MLS ((Z)-4-(4-methoxybenzylidene)-3-phenylisoxazol-5(4H)-one, $C_{17}H_{13}NO_3$) has been reported, and the crystal structure and the third-order NLO effect of DLS have been determined. [21] However, the structure of MLS and the second-order NLO properties for both crystals have not been examined yet. In this work, DLS and MLS crystals have been grown, and their second-order NLO properties have been reported for the first time. In addition, UV-vis absorption spectroscopy, thermal properties, transmission spectra, and solubility of DLS and MLS have also been investigated.

Experimental

Synthesis

All chemicals were purchased from commercial suppliers (Alfa Aesar, J&K Scientific, TCI Shanghai, and Sinopharm Chemical Reagent) and used without further purification. The two compounds were synthesized by condensations reaction from the corresponding aldehyde and isoxazolone in good yields.[23]

[a] Beijing Center for Crystal Research and Development, Key Laboratory of Functional Crystals and Laser Technology, Technical Institute of Physics and Chemistry, Chinese Academy of Sciences, Beijing 100190, China. E-mail: gczhang@mail.ipc.ac.cn
[b] University of Chinese Academy of Sciences, Beijing 100049, P.R. China

† Electronic Supplementary Information (ESI) available: Crystallographic data in CIF format for CCDC 1055698. See DOI: 10.1039/x0xx00000x

The chemical structures of the DLS and MLS molecule are shown in Fig. 1. 1H-NMR spectroscopy data were recorded on a Bruker Avance 400 Spectrometer in $CDCl_3$ solution.

DLS 1H NMR (400 MHz, $CDCl_3$) δ 8.40 (d, J = 8.7 Hz, 2H), 7.60 – 7.57 (m, 2H), 7.56 – 7.53 (m, 3H), 7.40 (s, 1H), 6.79 (d, J = 8.8 Hz, 2H), 3.17 (s, 6H).

MLS 1H NMR (400 MHz, $CDCl_3$) δ 8.42 (d, J = 8.9 Hz, 2H), 7.61 – 7.55 (m, 5H), 7.52 (s, 1H), 7.00 (t, J = 5.9 Hz, 2H), 3.92 (s, 3H).

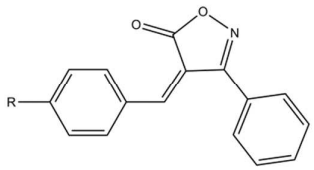

R	Abbr.
$-N(CH_3)_2$	DLS
$-OCH_3$	MLS

Fig. 1 Chemical structures of investigated molecules.

Single Crystal Growth and Solubility

DLS crystals were grown by evaporation in dichloromethane around 30℃. As shown by scanning electron microscopy (SEM) (Fig.2(a)), the micron DLS crystals are layered stacking with layer thickness about 10μm. The dark red bulk crystal with size of 5×5×0.8mm^3 and high optical quality was obtained, as seen in Fig. 2(b), and no hydrate phase was observed. The crystal size is adequate for optical experiments. In addition, in contrast to highly soluble ionic DAST crystals, non-ionic DLS crystals are not soluble in water, which avoid forming a centrosymmetric hydrated phase with water. Therefore, DLS crystals possess excellent environmental stability. Solubility of DLS in acetronitrile was measured between 30℃ and 55℃, which shows possibility for crystal growth by cooling method, as shown in Fig. S1.

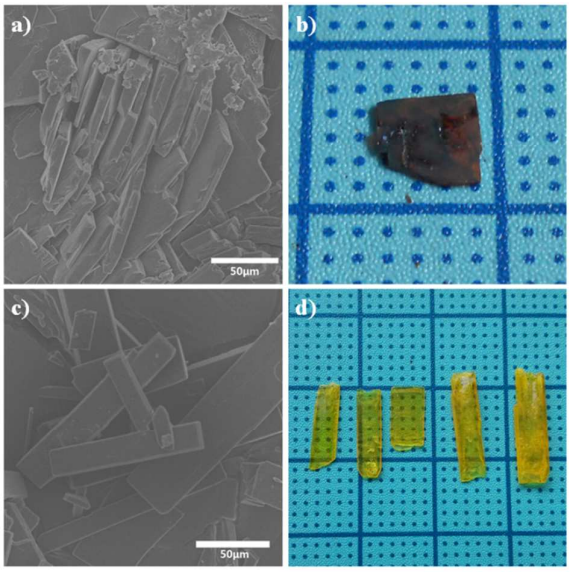

Fig. 2 (a) SEM images and (b) obtained bulk crystals of DLS. (c) SEM images and (d) obtained bulk crystals of MLS.

Solubility of MLS in acetronitrile was also measured (see Fig. S1), and MLS crystals were grown by cooling method. Crystalline powders of MLS were synthesized and purified through recrystallization before preparing MLS/acetonitrile saturation solution. Taken solubility into consideration, the cooling zone was from 45℃ to room temperature and the cooling rate was about 0.5℃/day. Crystal first nucleates appeared at about 41~40℃ and kept a quite fast growth rate. MLS crystals are of yellow color. SEM images (Fig.2(c)) shows that MLS crystals are rectangular bar with length about 80μm and width about 20μm and Fig. 2(d) shows the obtained bulk MLS crystals, with the size of (3-5)×(8-13)×(0.5-1) mm^3.

X-Ray structure determination

X-ray data were collected with graphite-monochromatized Mo Kα (λ = 0.71073 Å) on a Rigaku AFC10 diffractometer equipped with a Saturn CCD detector. The collection of the intensity data, cell refinement and data reduction were carried out with the use of the program Crystalclear.[24] The structures were solved with SHELXS-97 by a direct method and refined using SHELXL-97.[25] All of the hydrogen atoms were located on a difference Fourier map. The crystallographic data for the two crystals are listed in Table 1 and the relevant CIF files are given in the Supporting Information.

Table 1 Crystal data and structure refinements of DLS and MLS

	DLS[21]	DLS	MLS
formula	$C_{18}H_{16}N_2O_2$	$C_{18}H_{16}N_2O_2$	$C_{17}H_{13}NO_3$
f_w	292.33	292.33	279.28
crystal system	Monoclinic	Monoclinic	Orthorhombic
space group	*Cc*	*Cc*	*Pna2₁*
a (Å)	21.092(13)	21.112(11)	11.482(3)
b (Å)	6.521(3)	6.525(3)	6.0114(13)
c (Å)	12.149(7)	12.163(6)	19.382(5)
α (deg)	90.00	90.00	90.00
β (deg)	119.587(8)	119.582(5)	90.00
γ (deg)	90.00	90.00	90.00
V (Å^3)	1453.2(14)	1457.1(12)	1337.8(5)
Z	4	4	4
GOF on F^2	1.109	1.004	1.002
R_1 ($> 2\sigma(I)$)	0.0539	0.0397	0.0375
wR_2(all data)	0.1356	0.0906	0.0891
CCDC No.	947161	-	1055698

Characterizations

Scanning electron microscopy (SEM) was performed on HITACHI S-4800.

The UV-vis spectra in CH_2Cl_2 solution (1×10^{-5} mol/L) of the DLS and MLS were measured via Cary 1E UV−visible spectrophotometer.

Fluorescence microscopy was performed on Nikon c1 Si.

The thermal gravimetric analysis (TGA) was performed on a Perkin-Elmer Diamond TG/DTA spectrometer, and a heating rate of 10 °C min^{-1} in nitrogen was adopted.

The Cary 1E UV−visible spectrophotometer with a diffuse reflectance accessory was used to measure the spectra of DLS and MLS in the range of 250 nm (4.96 eV) - 1500 nm (0.83 eV).

The transmission spectra were measured using the Lambda 900 UV-vis-NIR spectrophotometer at room temperature in the range from 180 to 3000 nm.

Optical SHG tests of DLS and MLS were performed on the powder samples by means of the Kurtz-Perry method. Fundamental 2.09 μm light was generated with a Q-switched Ho:Tm:Cr:YAG laser. All the crystalline powders were prepared separately by mechanical grinding of single crystals, and particle size is sieved to same (0.2-0.3mm).

Computational Details

Quantum chemistry and first-principles calculation were adopted to investigate the optical nonlinearities of DLS and MLS. The quantum chemistry in B3LYP/6-311+G* level was implanted by Gaussian03 software. The first-principles electron structure calculations of DLS and MLS were performed by CASTEP, a plane-wave pseudopotential total-energy package based on density functional theory (DFT).[26] In the first-principles calculation, the functionals developed by Ceperley, Alder, Perdew，and Zunger in local density approximation (LDA) form were adopted to search the global minimum of the electron energy.[27] The interaction between valence electrons (C $2s^2 2p^2$, H $1s^1$, O $2s^2 2p^4$ and N $2s^2 2p^3$) and atom cores was modeled by optimized ultrasoft pseudopotential, which allow us to adopt a relatively small plane-wave basis set without compromising the computational accuracy.[28] The kinetic energy cutoff 300 eV and dense Monkhorst-Pack k-point meshes spanning less than 0.05 $Å^{-1}$ in the Brillouin zone were chosen.[29] Convergence test shows that these computational parameters are sufficiently accurate to determine the electron ground states.

Result and discussion

In the molecule structure of DLS, electron acceptor is 3-phenyl-5-isoxazolone, while electron donor is N, N-dimethylaniline, which are connected by π-conjugated C=C double bond. The obtained DLS crystal was confirmed to be identical to that in reference.[21] The crystallography data reveal that the DLS crystal has a noncentrosymmetric structure with monoclinic space group *Cc* and point group *m*. Molecule conformation of DLS exhibits good planarity between electron donor and acceptor, as seen in Fig. 3(a). The structure and spatial stacking pattern in DLS crystal are shown in Fig. 3(b). Along the *a* and *b* axis DLS molecules are parallel arranged, while along the *c* axis the main planes of the neighboring DLS molecules form an angle about 115°. As displayed in Fig. 3(c), main intermolecular interactions in DLS structure are originated from π-π interactions and hydrogen bonds, in which π-π interactions are dominant in the intermolecular interactions. Along the *b* axis, centroid distance between two adjacent parallel heterocyclic ring and phenyl ring (C(11)-C(16)) is 3.556(2) Å, and dihedral angle between these planes is 10.0°, while along the *c* axis, centroid distance and dihedral angle between heterocyclic ring and phenyl ring (C(1)-C(6)) belonged to unparalleled neighboring molecules is 3.712(2) Å and 5.87°, respectively. Thus, there are π-π interactions along both *b* and *c* axis.

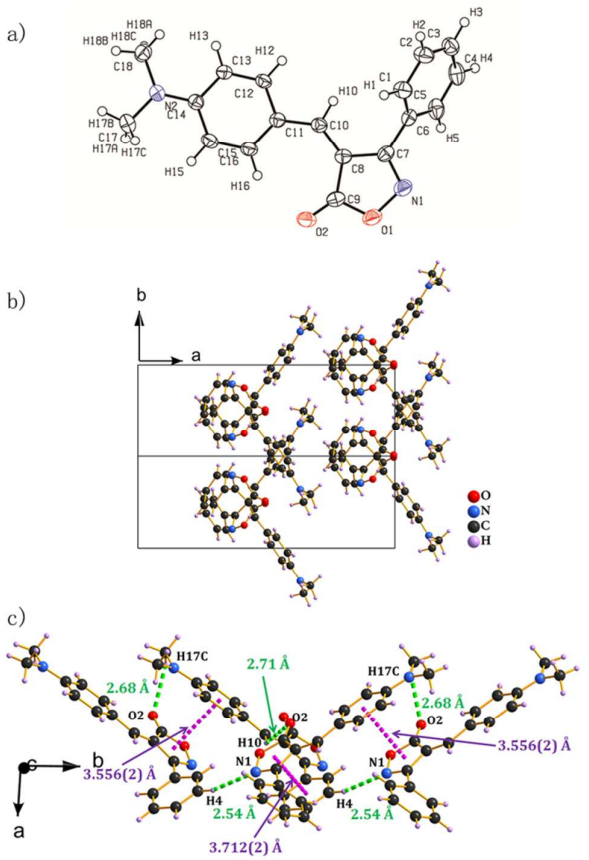

Fig. 3 (a) DLS molecule in crystalline state; (b) crystal structure of DLS along c axis; (c) intermolecular interactions between DLS molecules in crystalline state (purple dash lines for π-π interactions and green dash lines for hydrogen bonds).

In MLS molecule structure, electron acceptor is 3-phenyl-5-isoxazolone, while electron donor is methoxyl. MLS crystal also has noncentrosymmetric structure, with orthorhombic space group $Pna2_1$ and point group *mm2*. In crystalline state (Fig. 4(a)), the heterocyclic ring plane and the benzene plane (C(1)-C(6)) connected by alkene are almost in the same plane, with an angle about 5°, while the angle between heterocyclic ring and benzene plane (C(11)-C(16)) is 53°. The molecular structure and spatial stacking pattern in the MLS crystal are shown in Fig. 4(b). Adjacent MLS molecules along the *b* axis are parallel, while the adjacent molecules along the *a* or *c* axis are not completely parallel, which the angle between two molecule is about 114° along *a* axis and 50° along *c* axis. The intermolecular interactions between unparallel MLS molecule are rather complex, as seen in Fig. 4(c). One hydrogen bond is between N(1) on the heterocyclic ring and H(13) on the phenyl ring (C(11)-C(16)) of the neighboring MLS molecule, with N…H distance of 2.68 Å. Another is between O(2)…H(7) on alkene and O(2)…H(2) on the phenyl ring (C(1)-C(6)), with the distance of 2.62 Å and 2.64 Å, respectively. There are also π-π interactions in MLS crystal. Along the *b* axis, centroid distance between heterocyclic ring and (C(1)-C(6)) belonged to adjacent parallel molecules is 3.4466(12) Å and dihedral angle between these ring planes is 5.04°, while along *a* axis, centroid distance

and dihedral angle between heterocyclic ring and phenyl ring (C(11)-C(16)) belonged to unparalleled neighboring molecules is 3.6220(13) Å and 7.10°, respectively.

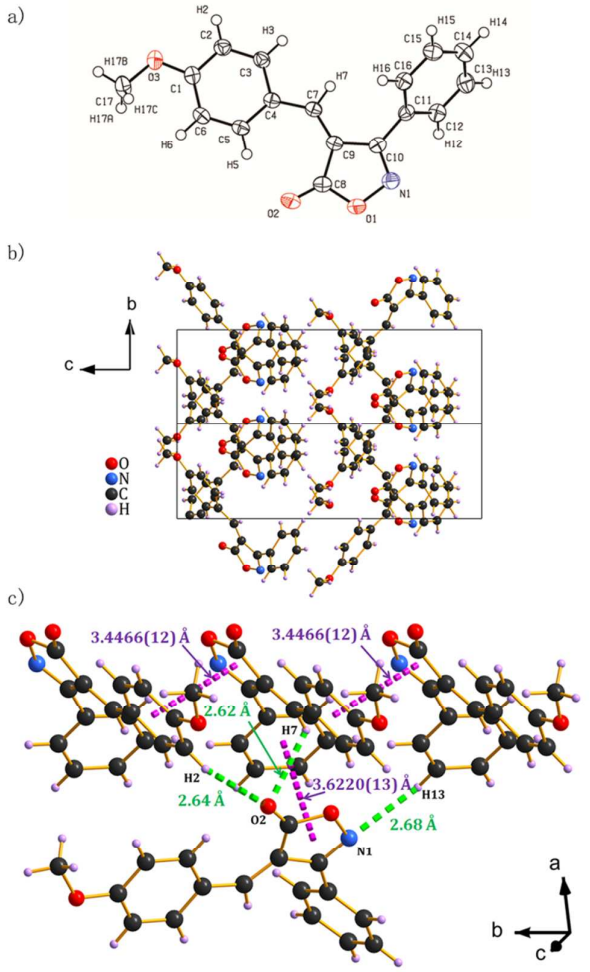

Fig. 4 (a) MLS molecule in crystalline state; (b) crystal structure of MLS along *a* axis; (c) intermolecular interactions between MLS molecules in crystalline state (purple dash lines for π-π interactions and green dash lines for hydrogen bonds).

In addition, intermolecular interactions affect the crystal morphology. As mentioned above, in DLS crystal structure, strong intermolecular interactions are along *b* and *c* axis, thus crystal growth rates along *b* and *c* axis are larger than *a* axis, consequently the main presence face of DLS crystals grown from dichloromethane is (100). Similarly in MLS crystal structure, as a result of strong intermolecular interactions along *a* and *b* axis, these two direction exhibit faster growth rates and finally form (001) as main presence face.

UV-vis absorption spectra and fluorescence microscopic images are presented in Fig.5 and Fig.6, respectively. The maximum absorption wavelengths (λ_{max}) of DLS and MLS in dichloromethane solution (1×10^{-5} M) are 478 nm and 388 nm, respectively and fluorescence microscopic images clearly shows that DLS and MLS are red emitters. According to the two-level model, the relative magnitude of first-order hyperpolarizabilities (β) is consistent with the order of λ_{max}.[30] Obviously, β (DLS) is larger than β (MLS), which resulted from stronger electron donor. Table S1 listed the calculated microscopic first-order hyperpolarizability in B3LYP/6-311+G* level using quantum chemistry method.[31] It confirmed that the microscopic first-order hyperpolarizability of DLS is larger than that of MLS. Fig. 7 displays the charge density maps obtained by the first-principles calculation. The electron clouds of DLS and MLS almost exhibit the same characterization. Both the donor group and acceptor group in the two compounds contribute to the SHG effect. The main difference concentrates on the C(14)-N(2) bonds in DLS and C(1)-O(3) bonds in MLS. The distribution of the electron cloud around C(14)-N(2) bond in DLS is more delocalized, while electron cloud around C(1)-O(3) bond in MLS is assembled around oxygen atom. This means that the C-N "tunnel" in DLS is more suitable for the charge transfer process compared with the C-O "tunnel" in MLS. Hence, DLS exhibits larger induced dipole moment and first-order hyperpolarizability in the same optical electric field[32], and DLS crystal may have larger macroscopic optical nonlinearities.

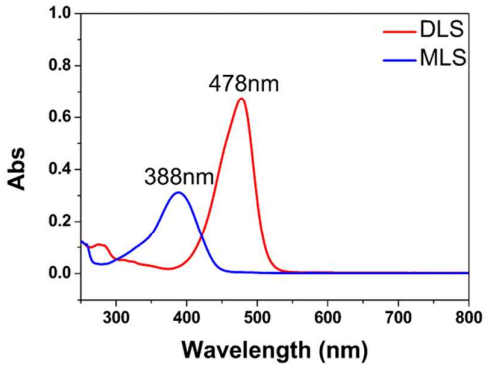

Fig. 5 UV-vis absorption spectra of DLS and MLS in dichloromethane solution (1×10^{-5} M)

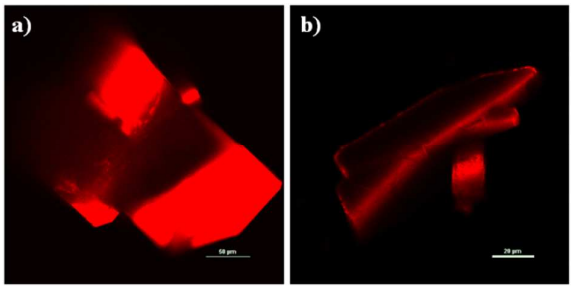

Fig. 6 Fluorescence microscopic images of (a) DLS and (b) MLS crystals excited with 408 nm light source.

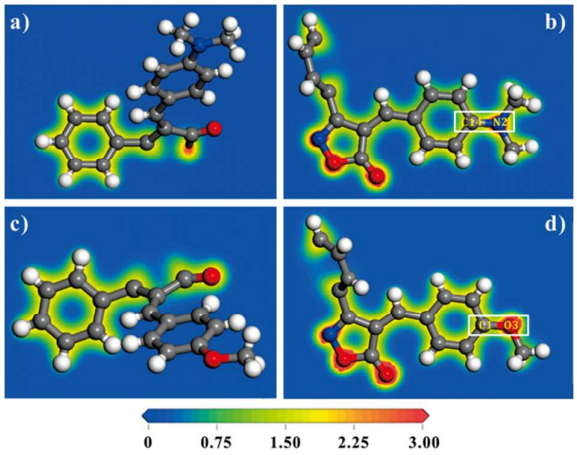

Fig. 7 The charge density maps around (a) phenyl ring (C(1)-C(6)), (b) molecule main plain in DLS, (c) phenyl ring (C(11)-C(16)) and (d) molecule main plain in MLS. The C, H, O and N atoms are represented by gray, white, blue, and red balls, respectively.

The powder SHG experiments [33] revealed that DLS and MLS have a pronounced SHG response with about 2.8 and 1.5 times that of the OH1 (2-(3-(4-hydroxystyryl)-5, 5-dimethylcyclohex-2-enylidene) malononitrile, d_{33} =120 ± 10pm/V, at 1.9 μm, hundreds times that of urea[34]), respectively, in the same size of 0.2-0.3 mm under 2.09 μm fundamental light (Fig. 8). Table S2 lists the SHG coefficients and SHG effect of the commonly used nonlinear crystals, and SHG intensity order is DAST≈DSTMS > DLS > MLS≈OH1. Thus, at present state, both DLS and MLS exhibit quite high reponse level. DLS and MLS are likely to possess large nonlinear coefficient and to be good candidates for NLO materials. The intense SHG responses from DLS and MLS crystals are mostly resulted from π-π interactions and dispersion, which are not found in OH1 crystal. As is well known, π-π interactions result in mutual polarizations of molecules, so the hyperpolarizability of DLS and MLS molecules in crystal phase can be strongly enhanced. [35, 36] Taken the dispersion in crystal phase into consideration[34], DLS and MLS have quite lower first exited energies (2.91 eV and 1.93 eV, respectively) compared with OH1 (3.14 eV), which show that dispersion for DLS and MLS crystal is more serious. Consequently, with the increasing of wavelength, the increasing magnitude of SHG coefficients is larger for DLS and MLS. The molecular spatial arrangements in the two crystal structure are in favor of the large SHG effects as well. DLS and MLS molecules are both in the almost same head-to-tail orientation, and thus the micro-nonlinearities are superposed and macroscopic nonlinearities are promoted. Therefore, the experimental SHG effects of DLS and MLS are reasonably larger than that of OH1 under 2.09 μm fundamental light.

The results of thermal gravimetric analysis (TGA) and differential scanning calorimetry (DSC) for the DLS and MLS crystals were shown in Fig. 9. The heating DSC curves of DLS and MLS clearly exhibit sharp endothermic peaks at 185 ℃ and 166 ℃, respectively, which indicate relatively moderate melting points (T_m). The initial weight-loss temperature (T_i) of DLS and MLS are about 253 ℃. So DLS and MLS crystals exhibit quite high thermal stability.

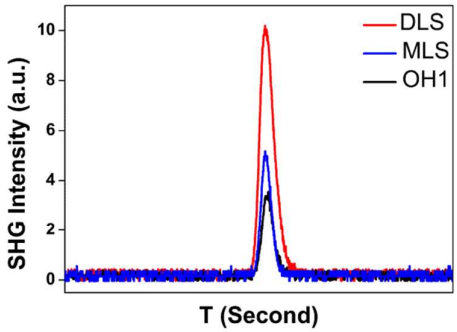

Fig. 8 Oscilloscope traces of the SHG signals of DLS, MLS and OH1 at the same particle size of 200–300 μm.

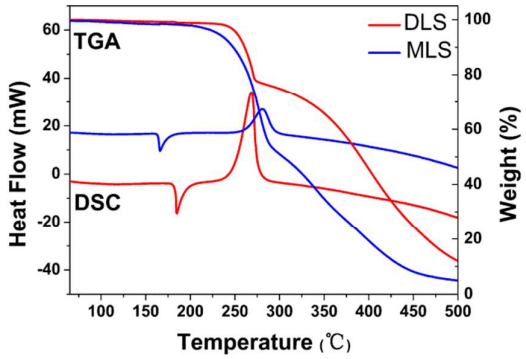

Fig. 9 Thermal analysis of DLS and MLS crystals.

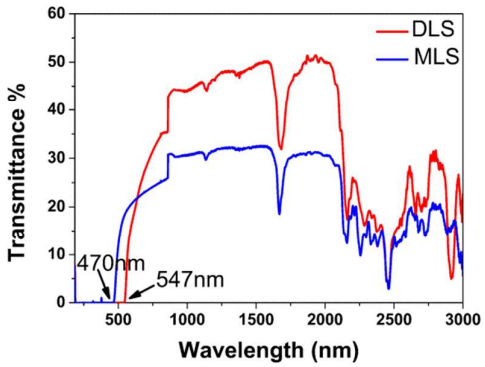

Fig. 10 Transmission spectra of DLS and MLS crystal plate.

DLS and MLS single crystals were obtained by slow evaporation in dichloromethane and slow cooling method in acetonitrile, separately. The unpolished *a*-plate (0.7 mm in thickness) of DLS and *c*-plate (0.5 mm in thickness) of MLS were used to measure transmission spectrum. As seen in Fig. 10, it is clear that the cut-off wavelengths of DLS and MLS

crystals are located at 547 nm and 470 nm, respectively, corresponding to the energy band gaps of 2.27 eV and 2.64 eV. Transparency regions of the two crystals range from 547 nm to 2170 nm and 470 nm to 2150 nm, respectively, except for the absorption bands observed in the infrared region at about 1.7μm, which correspond to C-H sketching vibration. Comparing with OH1, the two investigated crystals exhibit shorter cut-off wavelengths, wider transparency ranges, and less absorption bands, which make them advantageous for applications in the NIR region.[14]

Conclusions

In summary, DLS and MLS single crystals based on powerful electron acceptor 3-phenyl-5-isoxazolone were grown by slow evaporation method from dichloromethane and acetonitrile solution, respectively. Both DLS and MLS crystals possess noncentrosymmetric space group, which belong to monoclinic *Cc* and orthorhombic $Pna2_1$, respectively. In their crystal structures, π-π interactions and same head-to-tail orientation strongly enhance macroscopic nonlinearity, resulting in the strong SHG effect in DLS and MLS about 2.8 and 1.5 times that of OH1, respectively. Both DLS and MLS crystals show quite high thermal stability, and melting points are 185 ℃ and 166 ℃, respectively. Transparency regions range from 547 nm to 2170 nm for DLS and 470 nm to 2150 nm for MLS. The results imply that DLS and MLS may have the potential for NLO applications e.g., in the IR or even THz spectral region.

Acknowledgements

This work was supported by the National Natural Science Foundation of China (Grant No. 11174297) and China "863" project (Grant No. 2015AA034203).

Notes and references

‡ Chemical names for abbreviation: N-dimethylamino-N'-methylstilbazolium 4-methylbenzenesulfonate (DAST); N,N-dimethylamino-N'-methylstilbazolium 2,4,6-trimethylbenzenesulfonate (DSTMS); 4'-dimethylamino-n-methyl-4-stilbazolium p-chlorobenzenesulfonate (DASC); 4-dimethylamino-N'-methyl-4'-stilbazolium p-bromobenzenesulfonate (DASB); 4-N,N-dimethylamino-4'-N'-methyl-stilbazolium3-carboxy-4-hydroxybenzenesulfonate (DSCHS); (E)-4-(2-(5-(dimethylamino)thiophen-2-yl)vinyl)-1-methylpyridinium3-nitrobenzenesulfonate (TPNS); 2-(3-(4-hydroxystyryl)-5, 5-dimethylcyclohex-2-enylidene) malononitrile (OH1); 2-{3-[2-(4-dimethylaminophenyl)vinyl]-6,6-dimethylbicyclo[3.1.1]hex-2-enylidene}malononitrile(DAV1); 2-(5-methyl-3-(4-(pyrrolidin-1-yl)styryl)cyclohex-2 enylidene)malononitrile (MH2).

1 C. Diederichs, J. Tignon, G. Dasbach, C. Ciuti, A. Lemaitre, J. Bloch, P. Roussignol, C. Delalande, *Nature*, 2006, **440**, 904.
2 B. Ferguson, X. C. Zhang, *Nat. Mater*., 2002, **1**, 26.
3 S. R.Marder, J. W.Perry,C. P. Yakymyshyn, *Chem. Mater.*, 1994, **6**, 1137.
4 Z. Yang, L. Mutter, M. Stillhart, B. Ruiz, S. Aravazhi, M. Jazbinšek, A. Schneider, V. Gramlich, P. Günter, *Adv. Funct. Mater.,* 2007, **17**, 2018.
5 S. Brahadeeswaran, Y. Takahashi, M. Yoshimura, M. Tani, S. Okada, S. Nashima, Y. Mori, M. Hangyo, H. Ito, T. Sasaki, *Cryst. Growth Des.*, 2013, **13**, 415.
6 T. Matsukawa, T. Notake, K. Nawata, S. Inada, S. Okada, H. Minamide, *Opt. Mater.*, 2014, **36**, 1995.
7 J. H. Yin, L. Li, Z. Yang, M. Jazbinsek, X. T. Tao, P. Günter, H. Yang, *Dyes Pigments*, 2012, **94**, 120.
8 Y. Q. Dai, J. F. Tan, N. Ye, Z. Yang, *CrystEngComm*, 2014, **16**, 636.
9 O. P. Kwon, S. J. Kwon, M. Jazbinšek, F. D. J. Brunner, J. I. Seo, C. Hunziker, A. Schneider, H. Yun, Y. S. Lee, P. Günter，*Adv. Funct. Mater.*, 2008, **18**, 3242.
10 O. P. Kwon, S. J. Kwon, M. Stillhart, M. Jazbinšek, A. Schneider, V. Gramlich, P. Günter, *Cryst. Growth Des.*, 2007, **7**, 2517.
11 J. Y. Seo, S. B. Choi, M. Jazbinšek, F. Rotermund, P. Günter, O. P. Kwon, *Cryst. Growth Des.*, 2009, **9**, 5003.
12 Y. Li, J. X. Zhang, G. Q. Zhang, L. L. Wu, P. Z. Fu, Y. C. Wu, *J. Cryst. Growth*, 2011, **327**, 127.
13 P. X. Liu, D. G. Xu, Y. Li, X. Y. Zhang, Y. Y. Wang, J. Q. Yao, Y. C. Wu, *EPL.*, 2014, **106**, 60001.
14 Y. Li, Z. A. Wu, X. Y. Zhang, L. Wang, J. X. Zhang, Y. C. Wu, *J. Cryst. Growth*, 2014, **402**, 53.
15 M. Walther, K. Jensby, S. R. Keiding, H. Takahashi, H. Ito, *Opt. Lett.*, 2000, **25**, 911.
16 S. R. Marder, L. T. Cheng, B. G. Tiemann, A. C. Friedli, M. Blanchard-Desce, *Science*, 1994, **263**, 511.
17 J. D. Luo, J. l. Hua, J. G. Qin, J. Q. Cheng, Y. C. Shen, Z. H. Lu, P. Wang, C. Ye, *Chem. Commun.*, 2001, 171.
18 O. P. Kwon, B. Ruiz, A. Choubey, L. Mutter, A. Schneider, M. Jazbinšek, P. Günter, *Chem. Mater.*, 2006, **18**, 4049.
19 X. Y. Zhang, X. X Jiang, Y. Li, Z. S. Lin, G. C. Zhang, Y. C. Wu, *CrystEngComm*, 2015, **17**, 1050.
20 O. P. Kwon, S. J. Kwon, M. Jazbinšek, J. Y. Seo, J. T. Kim, J. I. Seo, Y. S. Lee, H. Yun and P. Günter, *Chem. Mater.*, 2011, **23**, 239.
21 D. Jiang, Z. Xue, Y. J. Li, H. B. Liu, W. S. Yang, *J. Mater. Chem. C*, 2013, **1**, 5694.
22 (a) A. Wahl, Meyer, Andre, *Compt. rend.* 1908, **146**, 638; (b) S. Fozooni, N. G. Hosseinzadeh, H. Hamidian, M. R. Akhgar, *J. Brazil. Chem. Soc.*, 2013, **24**, 1649.
23 M. Mirzazadeh, G. H. Mahdavinia, *E-Journal of Chemistry*, 2012, **9**, 425.
24 J. Rigaku Corporation: Tokyo, CrystalClear, 2008.
25 G. M. Sheldrick, *Acta Crystallogr*., Sect. A: Found. Crystallogr., 2008, **64**, 112.
26 (a) S. J. Clark, M. D. Segall, C. J. Pickard, P. J. Hasnip, M. J. Probert, K. Refson, M. C. Payne, *Z. Kristallogr*. 2005, **220**, 567. (b) M. C. Payne, M. P. Teter, D. C. Allan, T. A. Arias, J. D. Joannopoulos, *Rev. Mod. Phys*. 1992, **64**, 1045.
27 (a) J. P. Perdew, A. Zunger, *Phys. Rev. B*, 1981, **23**, 5048; (b) D. M. Ceperley, B. J. Alder, *Phys. Rev. Lett*. 1980, **45**, 566.
28 A. M. Rappe, K. M. Rabe, E. Kaxiras, J. D. Joannopoulos, *Phys. Rev. B*., 1990, **41**, 1227.
29 H. J. Monkhorst, J. D.Pack, *Phys. Rev. B*, 1976, **13**, 5188.
30 a) J. L. Oudar, D. S. Chemla, *J. Chem. Phys.*, 1977, **66**, 2664. b) J. L. Oudar, *J. Chem. Phys*. 1977, **67**, 446.
31 a) A. D. Becke, *J. Chem. Phys*. 1993, **98**, 5648. b) J. P. Perdew, *Phys. Rev. B,* 1986, **33**, 8822.
32 X. Jiang, S. Zhao, Z. Lin, J. Luo, P. D. Bristowe, X. Guan, C. Chen, *J. Mater. Chem. C*, 2014, **2**, 530.
33 S. K. Kurtz, T. T. Perry, *J. Appl. Phys.*, 1968, **39**, 3798.
34 C. Hunziker, S. J. Kwon, H. Figi, F. Juvalta, O. P. Kwon, M. Jazbinšek, P. Günter, *J. Opt. Soc. Am. B*, 2008, **25**,1678.

35 W. Zhang, A. F. Cozzolino, A. H. Mahmoudkhani, M. Tulumello, S. Mansour, I. Vargas-Baca, *J. Phys. Chem. B*, 2005, **109**, 18378.
36 A. Datta, S. K. Pati, *J. Chem. Phys.*, 2003, **118**, 8420.

Highlight

Two isoxazolone-based nonlinear crystals exhibit large SHG responses about 2.8 and 1.5 times that of OH1 respectively.